

1 **Technical note: Fu-Liou-Gu and Corti-Peter model performance evaluation for**
2 **radiative retrievals from cirrus clouds**

3

4 S. Lolli^{1,5}, J. R. Campbell², J. Lewis¹, Y. Gu³, E. J. Welton⁴

5 ¹NASA GSFC-JCET, Code 612, 20771 Greenbelt, MD, USA

6 ² Naval Research Laboratory, Monterey, CA, USA

7 ³ UCLA, Los Angeles, CA, USA

8 ⁴ NASA GSFC, Code 612, 20771 Greenbelt, MD, USA

9 ⁵ CNR-IMAA, Istituto di Metodologie per l'Analisi Ambientale, Potenza, Italy

10 *Corresponding author: simone.lolli@nasa.gov*

11 **Abstract**

12 We compare, for the first time, the performance of a simplified atmospheric
13 radiative transfer algorithm package, the Corti-Peter (CP) model, versus the more
14 complex Fu-Liou-Gu (FLG) model, for resolving top-of-the-atmosphere radiative
15 forcing characteristics from single layer cirrus clouds obtained from the NASA Micro
16 Pulse Lidar Network database in 2010 and 2011 at Singapore. Specifically, CP
17 simplifies calculation of clear-sky longwave radiation through regression analysis,
18 which contributes significantly to differences between the two. The results of the
19 intercomparison show that differences in annual net TOA cloud radiative forcing can
20 reach 68%. CP proves useful for first-order estimates of TOA cirrus cloud forcing,
21 but may not be suitable for quantitative accuracy, including the absolute sign of
22 cirrus cloud TOA forcing that can readily oscillate around zero globally.

23 **1. Introduction**

24 Cirrus clouds play a fundamental role in atmospheric radiation balance and their net
25 radiative effect remains unclear (IPCC 2013; Berry and Mace 2014; Campbell et al.
26 2016; Lolli et al. 2017). Feedbacks between cirrus dynamic, microphysical and
27 radiative processes are poorly understood, with ramifications across a host of
28 modeling interests and temporal/spatial scales (Liou 1985; Khvorostyanov and
29 Sassen 1998). Simply put, different models parameterize ice formation in varied, yet
30 relatively simplified, ways that impact how cirrus are resolved, and how their
31 macro/microphysical and radiative properties are coupled with other atmospheric
32 processes (e.g., Comstock et al. 2001; Immler et al. 2008). Consequently, models are
33 very sensitive to small changes in cirrus parameterization (Soden and Donner 1994;
34 Min et al. 2010; Dionisi et al., 2013).

35 Cirrus clouds are the only tropospheric cloud genus that either exerts a
36 positive or negative top-of-the-atmosphere (TOA) cloud radiative forcing effect
37 (CRE) during daytime. All other clouds exert a negative daytime TOA CRE. Cirrus
38 clouds exerting negative net TOA CRE cool the earth-atmosphere system and
39 surface below them. This occurs as the solar albedo term is greater than the
40 infrared absorption and re-emission term. Positive forcing occurs when the two are
41 reversed and infrared warming and re-emission exceed scattering back to space. In
42 contrast, all clouds cause a positive nighttime TOA value, with an infrared term
43 alone and no compensating solar albedo term. This dual property is what makes
44 cirrus distinct, and why it's crucial to understand how well radiative transfer
45 models are resolving TOA CRE properties.

46 The burgeoning satellite and ground-based era of atmospheric monitoring
47 (Sassen and Campbell 2001; Campbell et al. 2002; Welton et al. 2002; Nazaryan, et
48 al. 2008; Sassen et al. 2008) has led to a wealth of new data for looking at global
49 cirrus cloud properties. In particular, TOA CRE, or at the surface (SFC), are evaluated
50 by means of radiative transfer modeling, designed with different degrees of
51 complexity. What is not yet known is how the relative simplicity of some models
52 translates to a relative retrieval uncertainty, given that the CRE effect of cirrus
53 clouds, at both the ground and TOA, are typically on the order of 1 W m^{-2} . (e.g.,
54 Campbell et al. 2016; Lolli et al. 2017). Whereas some studies show the relative
55 uncertainty of such models as static percentages (Corti and Peter, 2009), the
56 absolute magnitude of uncertainty with respect to cirrus CRE is necessary to
57 understand whether or not they fit within acceptable tolerance thresholds sufficient
58 for quantitative use. Further, given the sensitivity in the sign of net annual cirrus
59 cloud TOA CRE specifically (Campbell et al. 2016), it's plausible that some simpler
60 models are routinely aliasing positive versus negative TOA CRE.

61 Corti and Peter (2009; CP) describe a simplified radiative transfer model that
62 relies upon a constrained number of input parameters, including surface
63 temperature, cloud top temperature, surface albedo, layer cloud optical depth, and
64 the solar zenith angle. CP simplifies drastically the framework of the Fu-Liou-Gu
65 radiative transfer model (Fu and Liou 1992; Gu et al. 2003; Gu et al., 2011; FLG), for
66 instance, through a parameterization of the longwave and shortwave fluxes derived
67 from the FLG model calculations for realistic atmospheric conditions. Moreover, CP
68 does not directly consider gaseous absorption. The model has increasingly been

69 used to assess cirrus cloud radiative effects (Kothe et al. 2011; Kienast-Sjögren et al.
70 2016; Burgeois et al. 2016) from lidar measurements, owing to its relative simplicity
71 and lower computational burden compared with a model like FLG.

72 To date, CP model performance vs. FLG model has been evaluated for
73 sensitivities only to simulated synthetic clouds and never on real measurements,
74 especially those collected over long periods (Corti and Peter 2009). Such evaluation,
75 however, can readily be conducted using the unique NASA Micro Pulse Lidar
76 Network (MPLNET; Welton et al. 2002; Campbell et al. 2002; Lolli et al. 2013; Lolli
77 et al., 2014), featuring instruments capable of continuously monitoring cloud optical
78 characteristics. The objective of this technical note is to then assess differences
79 between CP and FLG in terms of net annual TOA CRE. CP and FLG model
80 performance are evaluated using MPLNET datasets collected from Singapore in
81 2010 and 2011, a permanent tropical MPLNET observational site, and Greenbelt,
82 Maryland in 2012, a midlatitude site. Our goal is to more appropriately characterize
83 the sensitivities of CP relative to what is generally considered a more complex, and
84 presumably more accurate, model, with the hopes of better understanding relative
85 uncertainties, and thus interpreting whether such uncertainties are appropriate for
86 long-term global cirrus cloud analysis.

87

88 **2. Method**

89 FLG is a combination of the delta four-stream approximation for solar flux
90 calculations (Liou et al. 1988) and a delta-two-four-stream approximation for IR
91 flux calculations (Fu et al. 1997), divided into 6 and 12 bands, respectively. It has

92 been extensively used to assess net cirrus cloud daytime radiative effects, most
93 recently for daytime TOA forcing characteristics within MPLNET datasets (Campbell
94 et al. 2016; Lolli et al. 2017). The results from these studies have led to the
95 hypothesis of a meridional gradient in cirrus cloud daytime TOA radiative forcing
96 existing, with daytime cirrus clouds producing a positive daytime TOA CRE at lower
97 latitudes that reverses to a net negative daytime TOA CRE approaching the non-
98 snow and ice-covered Polar Regions. They estimate an absolute net cirrus daytime
99 TOA forcing term between 0.03 and 0.27 W m⁻² over land at a mid-latitude site,
100 which ranges annually between 2.198 - 2.592 W m⁻² at Singapore. The key here to
101 this phenomenon is the possible oscillation of the net TOA CRE term about zero,
102 which is believed to vary by a maximum +/- 3 W m⁻² in absolute terms (i.e.
103 normalized for relative cirrus cloud occurrence rate locally) after accounting for
104 polar clouds that should be net cooling elements and varying surface albedos over
105 land and water exclusively (i.e., not ice). Resolving such processes thus requires
106 relatively high accuracy in radiative transfer simulations.

107 To calculate daytime cirrus cloud radiative effects from MPLNET datasets,
108 the lidar-retrieved single layer cirrus cloud extinction profile (Campbell et al. 2016;
109 Lewis et al., 2016, Lolli et al., 2017) is transformed into crystal size diameter (using
110 the atmospheric temperature profile) and ice water content (*IWC*) profiles using the
111 parameterization proposed by Heymsfield et al. (2014). Those parameters, at each
112 range bin, are input into FLG. The thermodynamic atmospheric profiles, together
113 with ozone concentrations are obtained with a temporal resolution of +/- 3 hr, from
114 a meteorological reanalysis of the NASA Goddard Earth Observing System Model

115 Version 5.9.12 (GEOS-5). In contrast, for a given cloud case, the corresponding cloud
116 and atmospheric CP input parameters are explicitly the surface temperature, the
117 cloud top temperature, the surface albedo, the cloud optical depth for the specific
118 layer and the solar zenith angle.

119 Calculations here are performed for two MPLNET observational sites,
120 Singapore and Greenbelt, Maryland (i.e., NASA Goddard Space Flight Center; GSFC).
121 For the former site, two different values of the surface albedo, which is a common
122 input parameter in both models, are fixed at 0.12 and 0.05, respectively, as
123 Singapore is a metropolitan area completely surrounded by sea. This allows us to
124 more reasonably characterize forcing over the broader archipelago of Southeast
125 Asia, and follows the experiments described by Lolli et al. (2017). . At NASA GSFC,
126 only a single over-land albedo is used, though one that varies monthly between
127 0.12-0.15 based on climatology. Here we reconsider these results by first
128 intercomparing those solved with FLG and CP for net daytime TOA CRE over a
129 practical range of cloud optical depth (COD). As described in both Campbell et al.
130 (2016) and Lolli et al. (2017), daytime is specifically defined in these experiments as
131 those hours where incoming net solar energy exceeds that outgoing. Only under
132 such circumstances can the net TOA CRE term become negative. Otherwise, it is
133 effectively nighttime, as the term is positive and all clouds induce a warming TOA
134 term. Nighttime results will considered as context to understanding net diurnal
135 differences between the models when examining the GSFC dataset.

136

137 **3. Intercomparisons**

138 The yearly daytime cirrus net TOA CRE, normalized by corresponding
139 occurrence frequency, in this case as a function of COD, was evaluated at Singapore
140 (1.3 N, 103.8 E, 20 m above mean sea level) and GSFC (38.9 N, 76.8 W, 39m above
141 mean sea level) for both FLG and CP. The method to estimate MPLNET cirrus clouds
142 optical properties is described in Lewis et al. (2015) and Campbell et al. (2016), for
143 both 20 and 30 sr solutions from the unconstrained single-wavelength elastic lidar
144 equation (Campbell et al. 2016). For both models, the daytime cirrus cloud net TOA
145 CRE is calculated as the difference of two model computations using different
146 assumed states (cloudy sky minus cloud and aerosol particulate-free conditions) to
147 isolate the distinct cirrus cloud impact alone (in $W m^{-2}$).

148

149 *3.1 Model sensitivities*

150 An initial sensitivity study was carried out to evaluate how the input
151 parameters, and eventually their uncertainties, influence the net TOA CRE
152 calculations. Results are summarized in Table 1. Model input parameter
153 sensitivities were investigated for surface albedo, COD, earth surface temperature
154 and cloud top temperature. Table 1 shows how much the CRE changes by varying
155 each individual parameter alone. For instance, changing the surface albedo from
156 0.12 to 0.14 and keeping the other three parameters fixed produces a change of 22%
157 for CP model and 24% for FLG model. Changing COD from 1 to 1.1 produces a
158 change in CRE of 14% for CP and 18% for FLG. Changing surface temperature and
159 cloud top temperature of 1 K produces respective changes of 11% and 6% for CP

160 and 7% and 5% for FLG. Though subtle, the models exhibit some differences in
161 variance relative to the input parameters required to initialize them.

162

163 *3.2 Singapore 2010*

164 FLG and CP were compared over a total of 15039 daytime single layer cirrus
165 clouds at Singapore in 2010. Detailed consideration of how such a cloud sample is
166 resolved in Level 2 MPLNET datasets can be found in Lewis et al. (2016) and
167 Campbell et al. (2016). Figures 1, 2, 3 and 4 reflect histograms of cirrus cloud
168 relative frequency and net annual daytime TOA CRE normalized by corresponding
169 frequency, for both surface albedo values of 0.05 (Fig. 3 and 4; i.e., over sea) and
170 0.12 (Fig. 1 and 2; i.e. over land) at 0.03 COD resolution from 0 to 3. This latter
171 range was chosen as consistent with Sassen and Cho (1992), and the nominal
172 effective COD range corresponding with cirrus cloud occurrence. Note, since a
173 common cloud sample is used, the 20 sr samples vary in COD between only 0 and
174 approximately 1 in contrast to the 30 sr sample topping out at 3.

175 Intercomparison of net daytime TOA CRE vs. COD over the ocean at 20 sr
176 shows an overall forcing of 1.73 W m^{-2} for CP and 0.54 W m^{-2} for FLG. At 30 sr, we
177 obtain -0.17 W m^{-2} from CP and -0.10 W m^{-2} for FLG. The overall CP net TOA CRE is
178 greater in absolute magnitude than FLG by a maximum difference of 68%. This
179 value is obtained by taking the ratio between yearly CRE from FLG over CP and then
180 the percentage difference. Over land (urban environment), CP yearly net daytime
181 TOA CRE are higher than the FLG model by 41% (CP = 4.85 W m^{-2} , FLG= 2.85 W m^{-2}
182 at 20 sr; CP= 5.21 W m^{-2} and FLG= 2.36 W m^{-2} at 30 sr). The COD value at which

183 cirrus begin cooling the earth-atmosphere system, moving toward higher COD, is
184 systematically shifted towards higher values for CP with respect to FLG. This is
185 particularly evident over ocean at 20 sr where there is a shift of 0.2 in COD (0.6 for
186 CP and 0.4 for FLG; Fig. 3).

187

188 *3.3 Singapore 2011*

189 The same analysis was performed for the 2011 dataset, but during this year
190 the two models were intercompared over 18033 detected daytime cloud profiles.
191 Over ocean, CRE vs. COD results show a total net daytime TOA CRE of 1.01 W m^{-2} for
192 CP and 0.57 W m^{-2} for FLG at 20 sr, while at 30 sr the forcing is negative: -1.52 W m^{-2}
193 for CP and -0.52 W m^{-2} . The discrepancies in absolute magnitude are thus near 65%.
194 Over land, differences drop to 21% (CP = 3.90 W m^{-2} , FLG = 3.07 W m^{-2} at 20 sr; CP =
195 3.77 W m^{-2} and FLG = 3.32 W m^{-2} at 30%). Again it can be seen that there is a shift in
196 COD turning point value (0.65 COD for CP and 0.35 for FLG at 20 sr; Fig. 3).

197 To better understand the different outputs between the two models, a scatter
198 plot between from FLG barplot entries is shown in Figs. 2 and 4 (30 sr solution), and
199 the corresponding CP barplot values are plotted for each year, over land and over
200 ocean, in Figs. 5 and 6. The red line represents the actual linear data regression,
201 while the blue line represents an ideal case (i.e., slope=1, intercept=0). If the two
202 radiative transfer models show identical results regarding CRE, all the points should
203 lie on the blue line. The red line instead represents the actual regression line, or a
204 relative measure of how much the two models differ.

205 From Figs. 5 and 6, the FLG-derived net daytime TOA CRE of 1 W/m^2
206 corresponds with CP values ranging from 1.4 W/m^2 to 1.6 W/m^2 . This implies that
207 CP daytime TOA CRE values are systematically greater in absolute value than the
208 corresponding FLG values by 40%-60%. On the contrary, the bias (or the intercept
209 from the linear regression) shows higher variability depending on the year and
210 surface type underlying the cirrus cloud (land versus ocean). This indicates that
211 when a cirrus cloud shows a neutral effect (0 W/m^2) in FLG solutions radiative CP
212 calculations range from 0.02 to -1.5 W/m^2 , again depending on year and surface
213 albedo. This implies that characterization of cirrus cloud warming or cooling effects
214 must carefully be determined with these models.

215

216 *3.4 Greenbelt, Maryland 2010*

217 To limit potential assessment ambiguity based on a single-site analysis, we
218 performed a second model comparison using the 2010 NASA GSFC dataset. A
219 summary of this dataset and net daytime TOA CRE results can be found in Campbell
220 et al. (2016). As this site is land-locked, only the single albedo was, again, used,
221 though varied monthly based on climatological passive satellite estimates. 21107
222 daytime cirrus cloud profiles were considered. In Figure 7 is plotted the total net
223 TOA CRE vs. COD at 30 sr, for CP (-2.59 W/m^2) against FLG (0.05 W/m^2). A relative
224 differencing here is impractical. Suffice however, this is a significant difference, and
225 the sign of the net daytime forcing term is in direct question between the two.

226 With this NASA GSFC dataset, we further consider an additional 32185
227 nighttime cirrus cloud cases within the analysis (Fig. 7). The thought here is that,

228 relative to prior estimates of CP uncertainty compared with more complex models, a
229 diurnal average would be likely to produce a different, and plausibly closer, relative
230 agreement consistent with prior studies. That is, since during for most of the period
231 we define here as night there is no solar input, a simplification of the infrared
232 forcing terms and parameterizations alone would potentially yield a closer
233 comparison between the two models. For the NASA GSFC dataset, we solved net
234 nighttime TOA CRE of 29.1 W/m^2 with FLG compared with 21.0 W/m^2 with CP, or a
235 relative difference approaching 50%. This is a slightly lower than the Singapore
236 comparison, for example, but still higher than previously stated (Corti and Peter
237 2009). Table 2 summarizes the discrepancies in terms of CRE at both observational
238 sites.

239 It is useful at this point to discuss some of the potential elements driving
240 these differences. The larger discrepancies between the two models is likeliest
241 ascribed to the optimization of three specific parameters in the CP model: the first
242 two, σ^* and k^* (Eq. 2 of Corti and Peter, 2009) are respectively the approximated
243 values for the Stefan-Boltzmann constant and the surface temperature exponent
244 obtained from regression analysis and used to calculate the outgoing longwave
245 earth radiation. Instead, the last parameter, γ^* (again obtained from a regression
246 analysis), is related to the asymmetry factor and used to calculate the cloud
247 reflectance of shortwave radiation (Eq. 11 in Corti and Peter; 2009). We speculate
248 that, though the analysis is left to a future study on broader uncertainties in
249 modeling ice radiative properties inherently with any model, these parameters are

250 not the constants ascribed by CP, but that their values instead change with respect
251 to season and latitude.

252 The 20% relative accuracy claimed in Corti and Peter (2009) may be verified
253 for special conditions in tropical latitudes, where the three parameters discussed
254 above are well optimized. But, that is clearly not found from our study. Corti and
255 Peters (2009) expressly stated that they used fixed values for those three
256 parameters (again σ^* and k^* in Eq. 2 and γ^* in Eq. 11 in Corti e Peter, 2009) again
257 using regression analysis, but this shouldn't be the case, as net TOA CRF is very
258 sensitive to those parameters. For example, varying water vapor concentrations in
259 the atmosphere can be the responsible of a difference up to 25 W/m² (for
260 temperatures at the surface higher than 288K) in clear-sky earth longwave radiation
261 at Singapore, as stated in Corti and Peter (2009; Fig. 1). In our analysis we verified
262 that, over one year, the surface temperature is higher than 288K 66% of the time.
263 We advise that those looking to apply CP to long-term climate/cirrus cloud study
264 should carefully analyze the relevance of these settings to their given experiment
265 before directly applying the model.

266

267 **4. Conclusions**

268 Annual single-layer cirrus cloud top-of-the-atmosphere (TOA) radiative
269 effects (CRE) calculated from the Corti and Peter (2009) radiative transfer model
270 (CP) are compared with similar results from the more complex, and presumably
271 more accurate, Fu-Liou-Gu (FLG) radiative transfer model. The CP model calculates
272 CRE using a parameterization of longwave and shortwave fluxes that are derived

273 from real measurements optimized for a tropical environment. Values for these
274 parameterizations, as suggested in Corti and Peter (2009), lead to relative
275 differences in TOA CRE that far exceed the stated 20% in the original manuscript.
276 This includes parsing results out for daytime, nighttime or diurnal averages. It is
277 believed that these parameterizations cannot be considered global constants, as
278 originally defined for CP, but that they should be carefully evaluated on single case
279 basis for each experiment. Overall, CP uses less input parameters compared with
280 FLG, making it practically and computationally more efficient, particularly for large
281 climate datasets. This is the first time, however, that the two models are compared
282 using long-term cirrus clouds datasets, as opposed to synthetic datasets, with
283 experiments conducted using NASA Micro Pulse Lidar datasets collected at
284 Singapore in 2010 and 2011 (Lolli et al. 2017) and Greenbelt, Maryland in 2012.

285 More specifically, net daytime TOA CRE was evaluated versus cloud optical
286 depth (COD) for steps of 0.03 (COD range: 0-1) at 20 sr and for steps of 0.1 at 30 sr
287 (COD range: 0-3) for both the Singapore and Greenbelt, Maryland datasets. Our
288 findings suggest that the difference in annual net TOA CRE between the two models
289 approaches 68% in one experiment at Singapore. At Greenbelt, Maryland, the sign
290 of the net annual daytime TOA CRE term differs, and the absolute difference varies
291 between by nearly 2.5 W/m². Differences in the sign of the net TOA forcing term,
292 however, is most worrying. Since cirrus clouds are the only cloud that can exhibit
293 daytime positive or negative net TOA CRE, subtle differences in absolute magnitude
294 are less important than whether or not the clouds are inducing a cooling or forcing
295 term in the TOA radiation budget.

296 In spite of this comparison, even if we reasonably speculate that FLG is the
297 more accurate model overall, because of its relative complexity compared with CP,
298 we are still missing regular comparisons of FLG with real observational data. Thus,
299 the practical gains to long-term application of a simplified model like CP cannot be
300 overstated, given lower computational demands. However, we believe that the
301 results from this study are noteworthy because they show that the differences
302 between the two models are significant. With respect to cirrus annual net TOA CRE,
303 and given the perspective on their global distribution described by Campbell et al.
304 (2016) and Lolli et al. (2017), these sensitivities can lead to completely different
305 conclusions about global cirrus TOA forcing effects. Therefore, in future work, it is
306 imperative on the community to continue understanding and refining the global
307 parameterizations used in all radiative transfer models regarding cirrus. Continued
308 intercomparisons between models with real observation both at ground (using flux
309 measurements), in situ (aircraft measurements) and at TOA (using satellite-based
310 measurements,) remain critical interests. Further, dividing shortwave and longwave
311 bands to investigate whether or not there are wavelength selective differences in
312 CRE estimations between specific bands than currently recognized can improve our
313 analysis.

314

315 **Acknowledgements**

316 This study and the NASA Micro Pulse Lidar Network (MPLNET) are supported by
317 the NASA Radiation Sciences Program (H. Maring). Author JRC acknowledges the

318 Naval Research Laboratory Base Program and support of NASA Interagency

319 Agreement NNG15JA17P on behalf of MPLNET.

320

321

322 **References**

- 323 Berry, E., and G. G. Mace, 2014: Cloud properties and radiative effects of the Asian
324 summer monsoon derived from A-Train data. *J. Geophys. Res. Atmos.*, 119,
325 doi:10.1002/2014JD021458.
- 326 Bourgeois, Q. *et al.* 2016: Ubiquity and impact of thin mid-level clouds in the tropics.
327 *Nat. Commun.* 7:12432 doi: 10.1038/ncomms12432
- 328 Campbell, S. Lolli J. Lewis, Y. Gu, E. Welton, 2016 “Daytime Cirrus Cloud Top-of-
329 Atmosphere Radiative Forcing Properties at a Midlatitude Site and their
330 Global Consequence” *J. Applied Meteor. Climat.*,
331 <http://dx.doi.org/10.1175/JAMC-D-15-0217.1>
- 332 Campbell, et al., 2002,” “Aerosol Lidar Observation at Atmospheric Radiation
333 Measurement Program Sites: Instrument and Data Processing”, *J. Atmos.*
334 *Oceanic Technol.*, 19, 431-442
- 335 Comstock, J.M., T.P. Ackerson (2001), G. G. Mace;,”Cirrus radiative properties in the
336 tropical western pacific. *Eleventh ARM Science Team Meeting Proceedings*,
337 Atlanta, Georgia, March 19-23.
- 338 Corti, T. and Peter, T., 2009: “A simple model for cloud radiative forcing”, *Atmos.*
339 *Chem. Phys.*, 9, 5751-5758, doi:10.5194/acp-9-5751-2009
- 340 Dionisi, D., Keckhut, P., Liberti, G. L., Cardillo, F., and Congeduti, F., 2013: Midlatitude
341 cirrus classification at Rome Tor Vergata through a multichannel Raman-
342 Mie-Rayleigh lidar, *Atmos. Chem. Phys.*, 13, 11853-11868, doi:10.5194/acp-
343 13-11853-2013.

344 Fu, Q., K. N. Liou, 1992, "On the correlated *k*-distribution method for radiative
345 transfer in nonhomogeneous atmospheres", *J. Atmos. Sci.*, 49, 2139–2156,
346 1992.

347 Gu, Y., J. Farrara, K. N. Liou, and C. R. Mechoso, 2003: Parameterization of cloud-
348 radiation processes in the UCLA general circulation model. *J. Climate*, 16,
349 3357-3370.

350 Gu, Y., K. N. Liou, S. C. Ou, and R. Fovell, 2011: Cirrus cloud simulations using WRF
351 with improved radiation parameterization and increased vertical resolution.
352 *J. Geophys. Res.* 116, D06119, doi:10.1029/2010JD014574

353 Heymsfield, A., D. Winker, M. Avery, M. Vaughan, G. Diskin, M. Deng, V. Mitev, and R.
354 Matthey, 2014: Relationships between ice water content and volume
355 extinction coefficient from in situ observations for temperatures from 0° to
356 –86°C: Implications for spaceborne lidar retrievals. *J. Appl. Meteor. Climatol.*,
357 53, 479–505

358 Immler, F., Treffeisen, R., Engelbart, D., Krüger, K., and Schrems, O. 2008: "Cirrus,
359 contrails, and ice supersaturated regions in high pressure systems at
360 northern mid latitudes", *Atmos. Chem. Phys.*, 8, 1689-1699, doi:10.5194/acp-
361 8-1689-2008.

362 IPCC: Climate Change 2013 – The Physical Science Basis, Working Group I
363 Contribution to the Fifth Assessment Report of the Intergovernmental Panel
364 on Climate Change, edited by: Inter- governmental Panel on Climate Change,
365 Cambridge University Press, Cambridge, UK and New York, NY, USA, 2014.

366 Khvorostyanov V. I. and K. Sassen, 1998: Cirrus Cloud Simulation Using Explicit
367 Microphysics and Radiation. Part I: Model Description. J. Atmos. Sci., 55,
368 1808–1821

369 Kienast-Sjögren, E., Rolf, C., Seifert, P., Krieger, U. K., Luo, B. P., Krämer, M., and Peter,
370 T.: Climatological and radiative properties of midlatitude cirrus clouds
371 derived by automatic evaluation of lidar measurements, Atmos. Chem. Phys.,
372 16, 7605-7621, doi:10.5194/acp-16-7605-2016, 2016.

373 Kothe, S., Dobler, A., Beck, A. and Ahrens, B., 2011. The radiation budget in a regional
374 climate model. *Climate dynamics*, 36(5-6), pp.1023-1036.

375 Kuo-Nan Liou, 1986: Influence of Cirrus Clouds on Weather and Climate Processes:
376 A Global Perspective. Mon. Wea. Rev., 114, 1167–1199.

377 Lolli S., Campbell J. R, Lewis J. R, Gu Y., Marquis J., Chew B-N, Liew S-C, Salinas S.,
378 Welton E. J., 2017:” Daytime Top-of-the-Atmosphere Cirrus Cloud Radiative
379 Forcing Properties at Singapore” *J. of Applied. Met. and Climatology.*,
380 doi:10.1175/JAMC-D-16-0262.1, In press

381 Lolli S., J. Lewis, R. Campbell, Y. Gu, E. Welton, 2016, “Cirrus Cloud Radiative
382 Characteristics from Continuous MPLNET Profiling at GSFC in 2012”, *Óptica*
383 *pura y aplicada*, Vol. 49 (1), 1-6,doi:10.7149/OPA.49.1.1.

384 Lolli S. et al, 2013a, “Evaluating light rain drop size estimates from multiwavelength
385 micropulse lidar network profiling,”*J. Atmos. Oceanic Technol.*, **30**, 2798–
386 2807.

387 Lolli S. et al. 2014. “High Spectral Resolution Lidar and MPLNET Micro Pulse Lidar
388 aerosol optical property retrieval intercomparison during the 2012 7-SEAS

389 field campaign at Singapore.” *Proc. SPIE 9246, Lidar Technologies,*
390 *Techniques, and Measurements for Atmospheric Remote Sensing X*, 92460C
391 (October 20, 2014); doi:10.1117/12.2067812.

392 Lewis, J. R., J. R. Campbell, P. C. Haftings and E. J. Welton, 2015: Overview and
393 analysis of the MPLNET Version 3 cloud detection algorithm. *J. Atmos.*
394 *Oceanic Technol.*, submitted

395 Min, M., P. Wang, J. R. Campbell, X. Zong, and Y. Li, 2010, “Midlatitude cirrus cloud
396 radiative forcing over China”, *J. Geophys. Res.*, 115, D20210,
397 doi:[10.1029/2010JD014161](https://doi.org/10.1029/2010JD014161).

398 Nazaryan, H., M. P. McCormick, and W. P. Menzel, 2008, “Global characterization of
399 cirrus clouds using CALIPSO data”, *J. Geophys. Res.*, 113, D16211,
400 doi:[10.1029/2007JD009481](https://doi.org/10.1029/2007JD009481).

401 Sassen, K. and J. R. Campbell, 2001: A Midlatitude Cirrus Cloud Climatology from the
402 Facility for Atmospheric Remote Sensing. Part I: Macrophysical and Synoptic
403 Properties. *J. Atmos. Sci.*, 58, 481–496,

404 Sassen, K., Z. Wang, and D. Liu, 2008, “Global distribution of cirrus clouds from
405 CloudSat/Cloud-Aerosol Lidar and Infrared Pathfinder Satellite
406 Observations (CALIPSO) measurements”, *J. Geophys. Res.*, 113, D00A12,
407 doi:[10.1029/2008JD009972](https://doi.org/10.1029/2008JD009972).

408 Soden, B. J., and L. J. Donner (1994), Evaluation of a GCM cirrus parameterization
409 using satellite observations, *J. Geophys. Res.*, 99(D7), 14401–14413,
410 doi:[10.1029/94JD00963](https://doi.org/10.1029/94JD00963).

411 Welton, E. J., et al., 2002: Measurements of aerosol vertical profiles and optical
412 properties during INDOEX 1999 using micropulse lidars. *J. Geophys. Res.*,
413 107, 8019,
414

415 **FIGURES**

416

417 **FIGURE 1** Analysis over land (Albedo=0.12) for 20sr solution. Top Panel: CRE vs.
418 COD weighted by occurrence frequency for Corti and Peter(red) and FLG
419 (blue) models on 2011. Bottom Panel: CRE vs. COD weighted by
420 occurrence frequency for Corti and Peter(red) and FLG (blue) models on
421 2010

422

423 **FIGURE 2** Analysis over land (Albedo=0.12) for 30sr solution. Top Panel: CRE vs.
424 COD weighted by occurrence frequency for Corti and Peter(red) and FLG
425 (blue) models on 2011. Bottom Panel: CRE vs. COD weighted by
426 occurrence frequency for Corti and Peter(red) and FLG (blue) models on
427 2010

428

429 **FIGURE 3** Same as Figure 1, but over the ocean (Albedo=0.05)

430

431 **FIGURE 4** Same as Figure 2, but over the ocean (Albedo=0.05)

432

433 **FIGURE 5** Scatter plot and linear regression for 30sr solution for FLG and CP CRE in
434 2010 over land (upper panel) and ocean (lower panel)

435

436 **FIGURE 6** Scatter plot and linear regression for 30sr solution for FLG and CP CRE in
437 2011 over land (upper panel) and ocean (lower panel)

438

439 **FIGURE 7** Analysis on 2010 dataset from MPLNET GSFC observational site for 30sr
440 solution daytime (upper panel) and nighttime (lower panel).

441

442

443

444 Tables

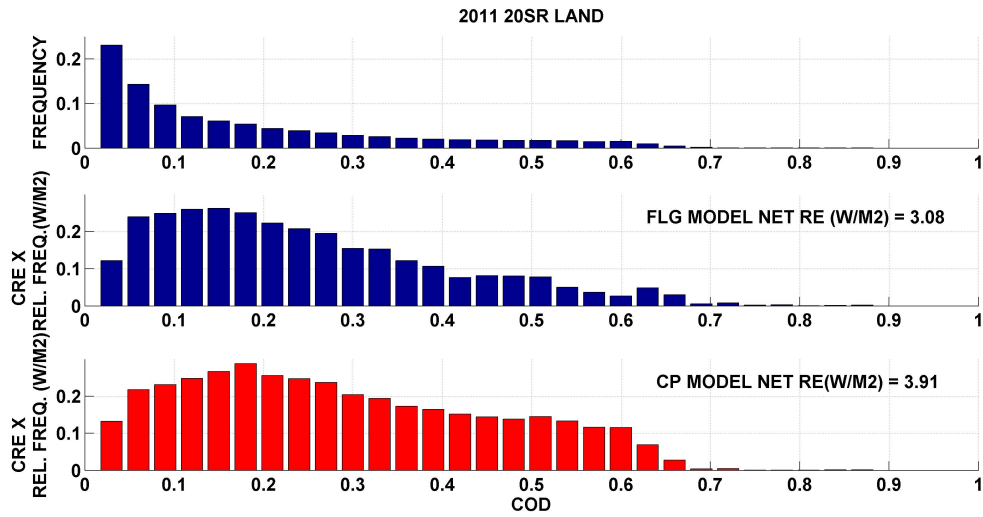
| | ALBEDO | COD | T surf | Cloud top T |
|------------|---------------|------------|---------------|--------------------|
| CP | 22% | 14% | 11% | 6% |
| FLG | 24% | 18% | 7% | 5% |

445 Table 1 Sensitivity of CP and FLG radiative transfer model with respect to the
 446 surface albedo, cloud optical depth (COD). Unperturbed parameters are COD=1,
 447 Surface albedo=0.12, Tsurf=294K Cloud top T=229K. The variation in net radiative
 448 forcing expressed in percentage for each parameter are calculated changing the
 449 surface albedo from 0.12 to 0.14, the COD from 1 to 1.1, and augmenting the
 450 temperatures of 1K.
 451

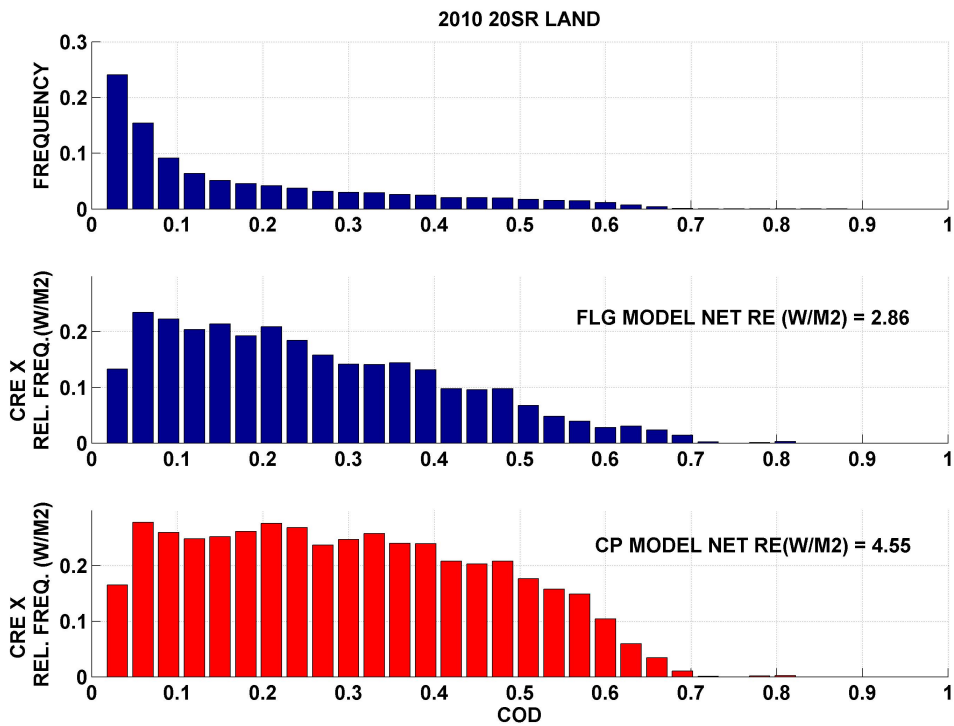
| CRE vs. COD | Land | Ocean |
|--------------------|-----------------------------|-------------------------------|
| SING 2010 | 20sr CP=4.85 FLG=2.85 (41%) | 20sr CP=1.73 FLG=0.54 (68%) |
| | 30sr CP=5.21 FLG=3.36 (35%) | 30sr CP=-0.17FLG=-0.09 (40%) |
| SING 2011 | 20sr CP=3.90 FLG=3.07 (21%) | 20sr CP=1.01 FLG=0.43 (57%) |
| | 30sr CP=3.77 FLG=3.32 (12%) | 30sr CP=-1.52 FLG=-0.52 (65%) |
| GSFC 2010 | 30sr CP=-2.59 FLG=0.05 | |

452 Table 2 Summary of principal CRE (W/m²) differences between FLG and CP
 453 radiative transfer model depending on year and on land/ocean.
 454

455 Figures



456



457

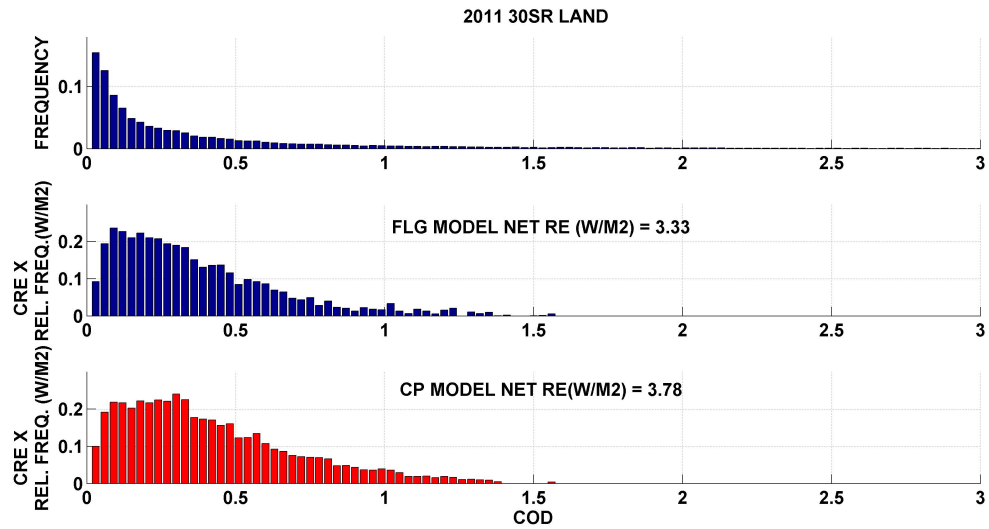
458 **Figure 1** Analysis over land (Albedo=0.12) for 20sr solution. Top Panel: CRE vs. COD weighted by
459 occurrence frequency for Corti and Peter(red) and FLG (blue) models on 2011. Bottom Panel: CRE vs.
460 COD weighted by occurrence frequency for Corti and Peter(red) and FLG (blue) models on 2010
461

462

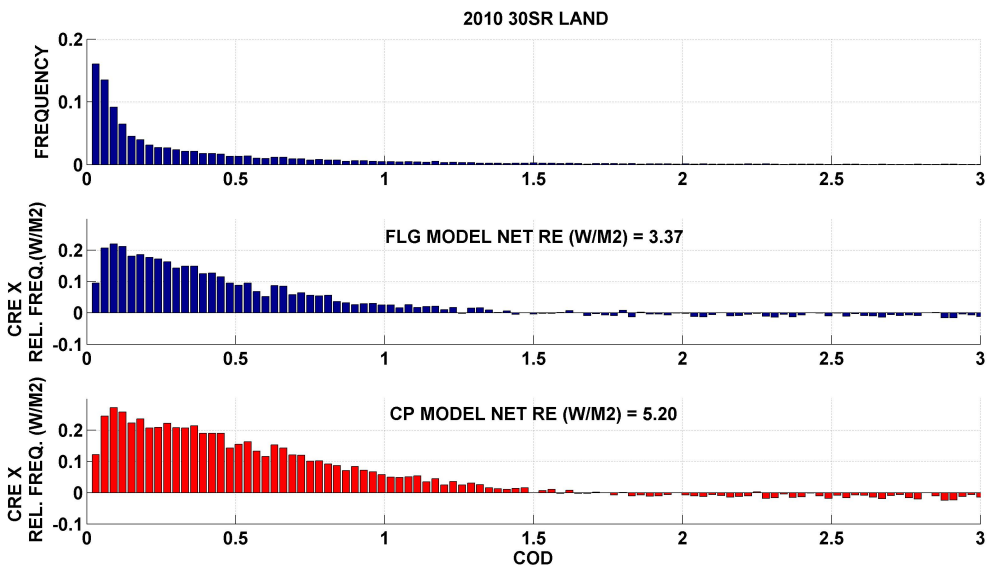
463

464

465

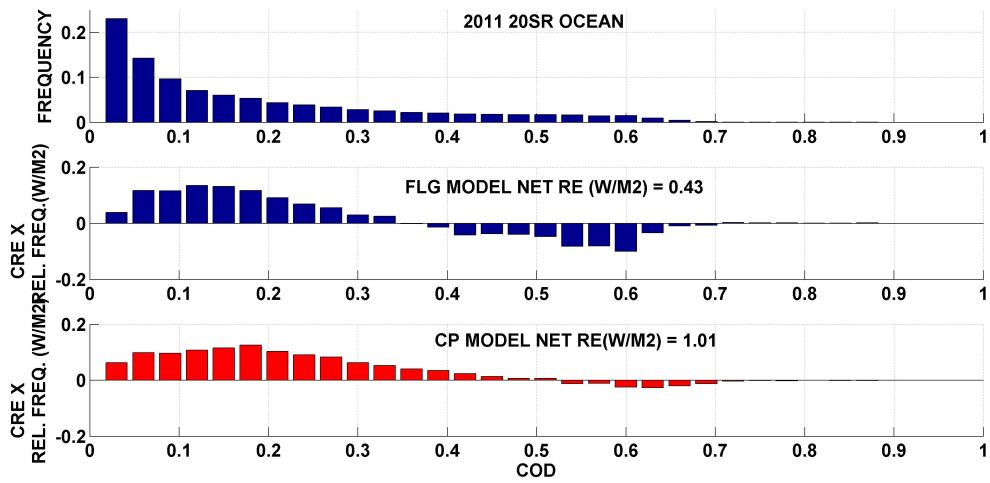


466

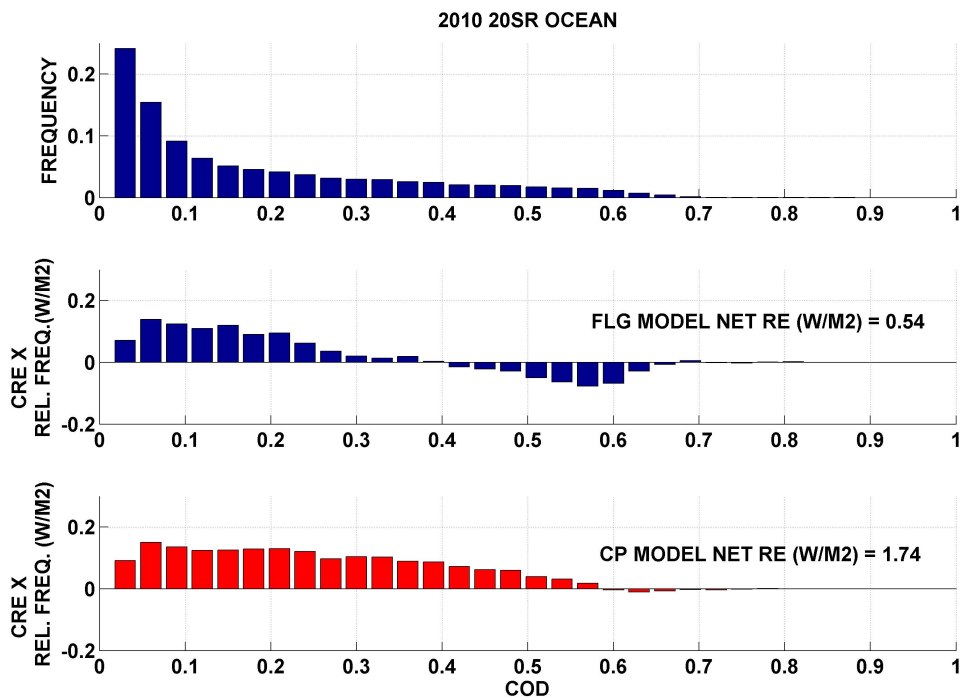


467

468 **Figure 2** Analysis over land (Albedo=0.12) for 30sr solution. Top Panel: CRE vs. COD weighted by
469 occurrence frequency for Corti and Peter(red) and FLG (blue) models on 2011. Bottom Panel: CRE vs.
470 COD weighted by occurrence frequency for Corti and Peter(red) and FLG (blue) models on 2010
471



472

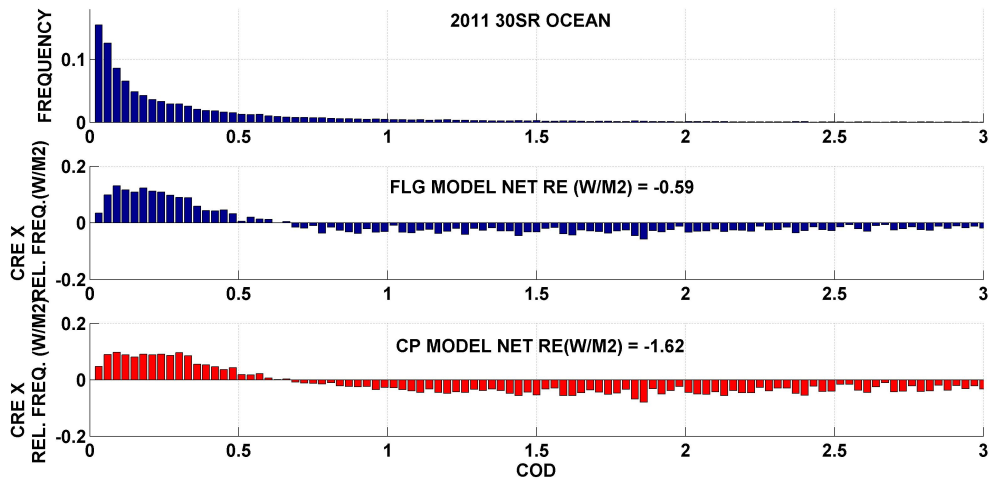


473

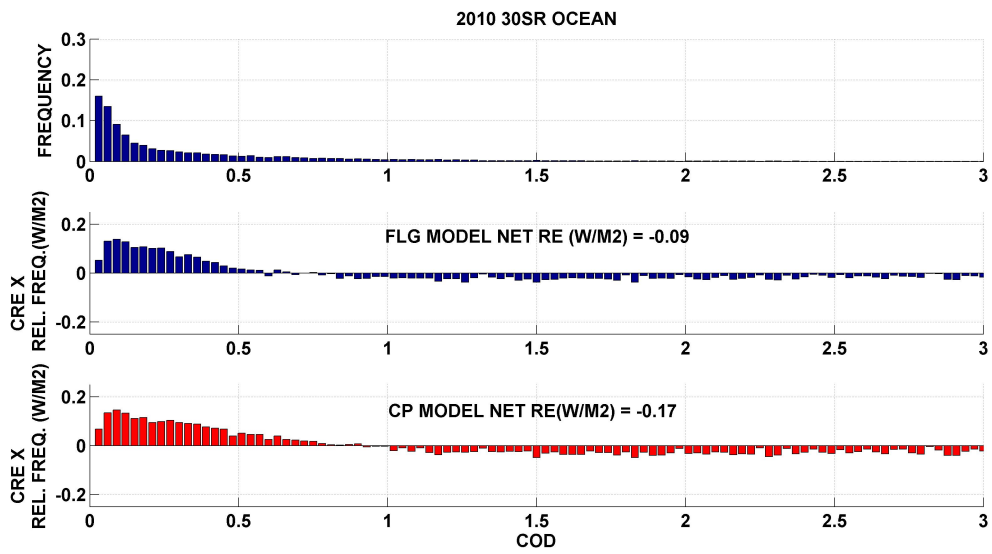
474 **Figure 3** Same as Figure 1, but over the ocean (Albedo=0.05)

475

476



477

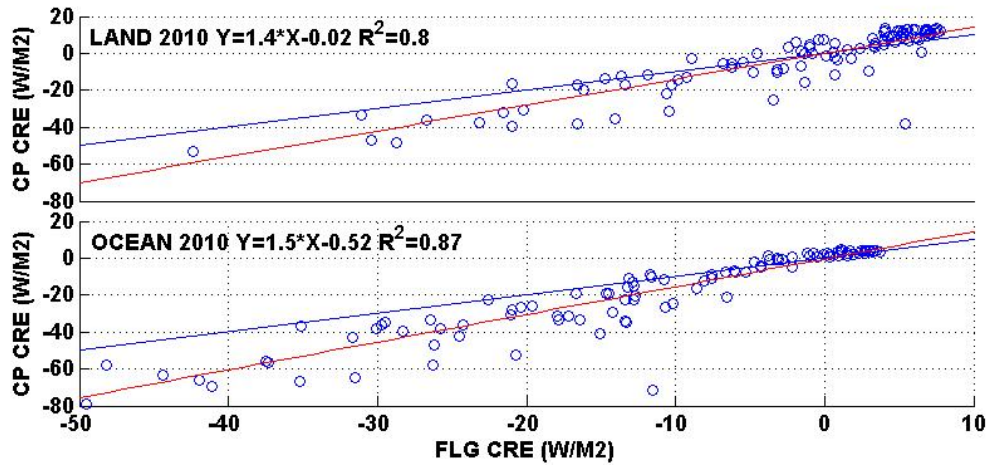


478

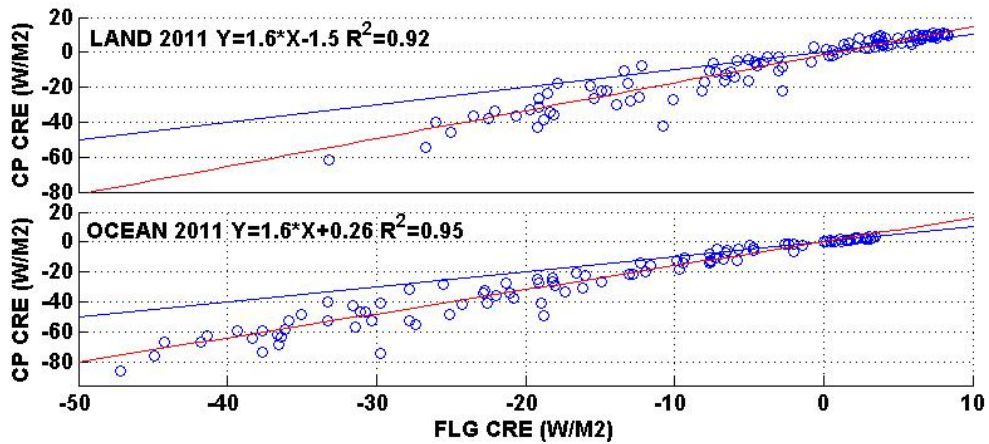
479

480

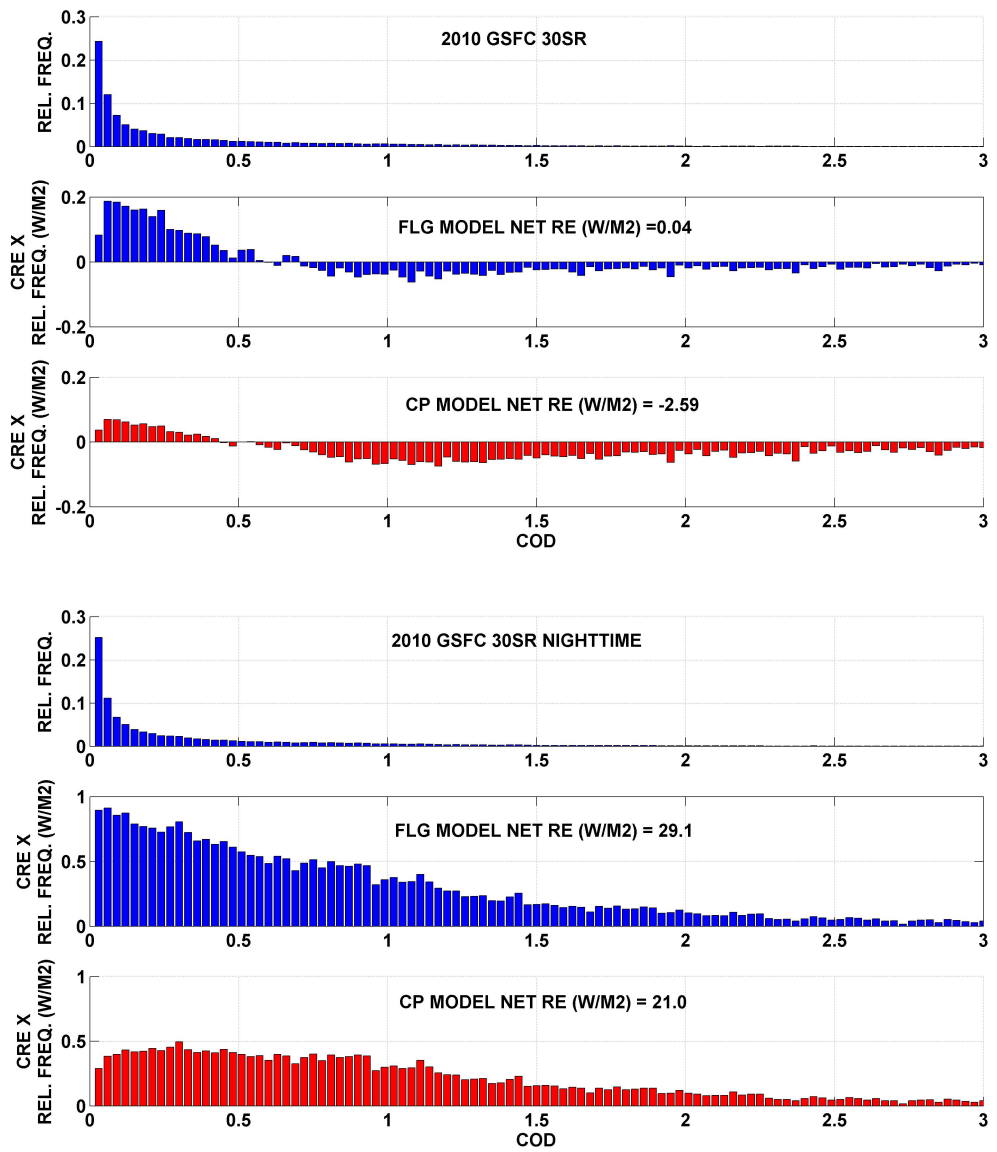
Figure 4 Same as Figure 2, but over the ocean (Albedo=0.05)



481 **Figure 5** Scatter plot and linear regression for 30sr solution for FLG and CP CRE in 2010 over land
 482 (upper panel) and ocean (lower panel)
 483



484 **Figure 6** Scatter plot and linear regression for 30sr solution for FLG and CP CRE in 2011 over land
 485 (upper panel) and ocean (lower panel)
 486
 487
 488
 489



490

491
 492
 493
 494
 495

Figure 7 Analysis on 2010 dataset from MPLNET GSFC observational site for 30sr solution daytime (upper panel) and nighttime (lower panel).